



HAL
open science

RELATIVISTIC BAND STRUCTURE OF GeTe, SnTe, PbTe, PbSe, AND PbS

Frank Herman, Richard Kortum, Irene Ortenburger, John P. van Dyke

► **To cite this version:**

Frank Herman, Richard Kortum, Irene Ortenburger, John P. van Dyke. RELATIVISTIC BAND STRUCTURE OF GeTe, SnTe, PbTe, PbSe, AND PbS. Journal de Physique Colloques, 1968, 29 (C4), pp.C4-62-C4-77. 10.1051/jphyscol:1968410 . jpa-00213614

HAL Id: jpa-00213614

<https://hal.science/jpa-00213614>

Submitted on 4 Feb 2008

HAL is a multi-disciplinary open access archive for the deposit and dissemination of scientific research documents, whether they are published or not. The documents may come from teaching and research institutions in France or abroad, or from public or private research centers.

L'archive ouverte pluridisciplinaire **HAL**, est destinée au dépôt et à la diffusion de documents scientifiques de niveau recherche, publiés ou non, émanant des établissements d'enseignement et de recherche français ou étrangers, des laboratoires publics ou privés.

RELATIVISTIC BAND STRUCTURE OF GeTe, SnTe, PbTe, PbSe, AND PbS (*)

Frank HERMAN, Richard L. KORTUM, Irene B. ORTENBURGER and John P. VAN DYKE

Lockheed Palo Alto Research Laboratory, Palo Alto, California

Résumé. — Les calculs relativistes de bandes par la méthode des ondes planes orthogonalisées ont été menés à bien aux points de symétrie simple dans la zone réduite de Brillouin pour plusieurs composés IV-VI. La structure de bande dans le reste de la zone a été déduite par interpolation. A notre connaissance, ce sont les premiers calculs de bandes pour les composés IV-VI qui se basent au départ sur des principes relativistes (contrairement aux calculs non relativistes affinés par des corrections relativistes et de couplage spin-orbite). Nos calculs conduisent à des modèles de bandes ayant une réalité physique, qui sont suffisamment précis pour tenir compte de la plupart des singularités des spectres expérimentaux de réflectivité. Il est difficile d'interpréter les spectres d'électro-réflexivité sans ambiguïté à l'aide de ces modèles de bande mais un certain nombre de recouvrements plausibles dans les spectres peuvent être faits.

Des calculs des bandes d'énergie et de spectre optique plus élaborés se poursuivent et seront publiés ailleurs.

Abstract. — Relativistic OPW band calculations have been carried out at key points in the reduced zone for several IV-VI compounds. The band structure in the remainder of the zone has been filled in with the aid of an interpolation scheme. To our knowledge, these are the first fully relativistic first-principles band calculations for IV-VI compounds (in contrast to non-relativistic calculations supplemented by relativistic and spin-orbit coupling corrections). Our first-principles band calculations lead to physically realistic energy band models which are sufficiently accurate to account for most of the characteristic features of the experimental reflectivity spectra. It is difficult to interpret the electroreflectivity spectra unambiguously in terms of these band models but a number of plausible spectral assignments can be made. Refined energy band and optical spectrum calculations are in progress and will be reported elsewhere.

I. Introduction. — During the past 15 years, an enormous amount of experimental and theoretical effort has been devoted to the study of the energy band structure (and related properties) of the IV-VI semi-conducting compounds, particularly PbS, PbSe, PbTe, SnTe, GeTe, and their alloys. As a result of this effort, we now know a great deal about the principal band edges (highest valence band maxima and lowest conduction band minima) of these materials. We also have a good qualitative idea of the overall form of the band structure throughout the reduced zone over an energy range of several eV. Recent summaries of the vast literature on the lead salts include those by Putley [1] and Prakash [2].

Much of our theoretical understanding of the principal band edges stems from the analyses of Dimmock and Wright [3] Cuff et al., [4], and Mitchell and Wallis [5]. Further insight into the nature of the band edges and information concerning the remainder of the band structure are provided by the first-principles APW band calculations of Johnson et al., [6], Conklin et al., [7], Ferreira, [8] and Rabii [9], and by the empirical pseudo-potential band calculations of Lin and Kleinman [10], Lin et al., [11] and Cohen et al. [12].

In spite of all the work that has already been done on the band structure of the IV-VI compounds, our knowledge is still incomplete, and many important questions remain to be answered. Though it is generally believed that the symmetry classification of the principal band edges in some of the IV-VI compounds is known, the evidence in some cases is rather circumstantial, and it would be reassuring to have more definite experimental or theoretical evidence to clinch the matter. It would also be highly desirable to have more

(*) The research reported in this paper was sponsored in part by the Lockheed Independent Research Fund; in part by the Air Force Cambridge Research Laboratories, Office of Aerospace Research, under Contract No. AF 19 (628)-5750; and in part by the Aerospace Research Laboratories, Office of Aerospace Research, under Contract No. F 33615-67-C-1793.

precise information about subsidiary valence and conduction band edges in the various IV-VI compounds as well as more accurate pictures of the overall band structures. In all of these domains, more precise information would put an end to current speculations and greatly accelerate progress in the correlation of experiment and theory.

With a view toward obtaining improved energy band pictures for the IV-VI compounds, we have carried out fully relativistic OPW energy band calculations for GeTe, SnTe, PbTe, PbSe, and PbS at a number of key points in the reduced zone, including Γ , X , L , and Σ ($\frac{1}{2}$ $\frac{1}{2}$ 0). The band structure in the remainder of the zone was then mapped out with the aid of an interpolation scheme. The resulting energy band pictures appear to be more realistic than those given by earlier band calculations. In this paper we will outline our approach and report some of our results; further results, including empirically-refined first-principles solutions, still more precise energy band pictures, and optical spectrum calculations will be presented in a subsequent publication [13].

II. Non-relativistic OPW energy band calculations. —

For purposes of orientation, non-relativistic OPW band calculations were carried out for GeTe, SnTe, PbTe, PbSe, and PbS using 181 OPWs at the zone center and a similar number of OPWs at other points in the reduced zone. As in other recent OPW band calculations [14-21] the trial crystal potential was represented by a spatial superposition of overlapping atomic potentials. The calculations were first carried out using non-relativistic self-consistent neutral atom potentials based on the Slater free-electron exchange approximation; the computations were then repeated using the Kohn-Sham version of this approximation. Representative results for both versions are listed in table I in the E (NREL) columns.

Although both exchange models give qualitatively similar band structures, the Slater model leads to somewhat larger energy separations between valence and conduction bands in some regions. (This statement is also true for the relativistic calculations which will be discussed later.) In view of the exploratory nature of these non-relativistic calculations, we decided not to iterate the solutions so as to obtain self-consistent crystal potentials and energy band structures, as we have done for other semiconductors [14-16].

III. Relativistic OPW energy band calculations. —

It has been recognized for some time that the neglect of relativistic [6, 22] and spin-orbit coupling effects [23] can lead to serious errors in first-principles band cal-

culations, particularly for crystals composed of heavy atoms, such as lead and mercury compounds. However, even in crystals such as Ge, the relativistic (mass-velocity and Darwin) corrections [6, 22] are quite substantial: the relativistic correction for the direct band gap of Ge is just about as large as the direct band gap itself (0.8 eV) [20].

One way of taking relativistic and spin-orbit coupling effects into account (within the framework of non-relativistic band calculations) is by first-order perturbation theory. This is the approach used in the earlier APW band calculations for the lead salts, [6-9] and in our own earlier OPW band calculations for a variety of crystals [14-18].

A more rigorous and physically satisfying approach involves carrying through all the calculations within a relativistic framework [24, 25]. Once the relativistic computer codes are developed, it is just as easy, and only slightly more expensive, to perform fully relativistic band calculations rather than non-relativistic band calculations supplemented by perturbation corrections. We have already studied over 25 different crystals using both approaches, and over 25 additional crystals (mostly composed of the lighter atoms) using the non-relativistic-perturbation approach only [20].

Our relativistic band calculations are based on Soven's relativistic formulation [25] of the OPW method, but our choice of crystal potential differs considerably from Soven's. In contrast to Soven — who was primarily interested in metallic crystals such as thallium — our relativistic trial potential is represented by a spatial superposition of overlapping atomic potentials (just as in the non-relativistic case), and this crystal potential is used for core, valence, and conduction band states alike. In the present context, we use relativistic self-consistent atomic potentials of the Slater or Kohn-Sham free-electron exchange type [26] rather than their non-relativistic counterparts, [27] as before. To insure the same high degree of convergence as in our non-relativistic calculations, the same number of OPWs is used now as before (e. g., 181 OPWs at the zone center).

We have rederived Soven's expression for the relativistic OPW matrix elements and reduced all of these to forms involving radial integrals (Ref. [25] does not contain the fully reduced forms). In the Appendix, we outline the essential features of the relativistic OPW method, and then we write down the fully reduced expressions for the various matrix elements. The Appendix should be of particular interest to those planning first-principles or parametrically-simulated relativistic OPW band calculations.

TABLE I

Electronic energy levels for GeTe, SnTe, PbTe, PbSe, and PbS based on non-relativistic OPW band calculations [E (NREL)]. The reduced relativistic scheme E^* (REL) based on Slater exchange is also shown. All entries are in eV.

| Level | GeTe | | | SnTe | | | PbTe | | | PbSe | | | PbS | | | Level |
|---------------|--------------------|-----------------|-----------------|--------------------|-----------------|-----------------|--------------------|-----------------|-----------------|--------------------|-----------------|-----------------|--------------------|-----------------|-----------------|----------------|
| | Kohn-Sham exchange | Slater exchange | Slater exchange | Kohn-Sham exchange | Slater exchange | Slater exchange | Kohn-Sham exchange | Slater exchange | Slater exchange | Kohn-Sham exchange | Slater exchange | Slater exchange | Kohn-Sham exchange | Slater exchange | Slater exchange | |
| | E (NREL) | E (NREL) | E^* (REL) | E (NREL) | E (NREL) | E^* (REL) | E (NREL) | E (NREL) | E^* (REL) | E (NREL) | E (NREL) | E^* (REL) | E (NREL) | E (NREL) | E^* (REL) | |
| $\Gamma_{2'}$ | 9.0 | 10.0 | 10.1 | 8.4 | 9.6 | 9.6 | 8.2 | 9.4 | 9.7 | 9.8 | 11.4 | 11.3 | 10.7 | 12.5 | 12.3 | $\Gamma_{2'}$ |
| Γ_{12} | 8.6 | 8.8 | 9.0 | 8.2 | 8.5 | 8.8 | 8.3 | 8.6 | 8.9 | 10.0 | 10.6 | 10.7 | 10.8 | 11.6 | 11.4 | Γ_{12} |
| Γ_1 | 10.4 | 10.8 | 10.0 | 10.5 | 11.0 | 10.0 | 10.6 | 11.2 | 9.1 | 12.5 | 13.5 | 10.8 | 14.3 | 15.3 | 11.8 | Γ_1 |
| Γ_{25} | 6.4 | 6.9 | 7.0 | 6.2 | 6.8 | 6.9 | 6.3 | 6.9 | 7.2 | 7.8 | 8.7 | 8.8 | 8.5 | 9.6 | 9.5 | $\Gamma_{12'}$ |
| Γ_{15} | 5.3 | 5.3 | 5.2 | 5.6 | 5.9 | 5.6 | 5.9 | 6.2 | 5.6 | 7.4 | 8.1 | 7.3 | 8.5 | 9.4 | 8.0 | Γ_{15} |
| Γ_{15} | 0.0 | 0.0 | 0.0 | 0.0 | 0.0 | 0.0 | 0.0 | 0.0 | 0.0 | 0.0 | 0.0 | 0.0 | 0.0 | 0.0 | 0.0 | Γ_{15} |
| Γ_1 | -1.8 | -2.3 | -3.6 | -0.8 | -1.1 | -2.8 | -0.6 | -0.9 | -4.2 | -1.2 | -0.8 | -3.9 | -0.7 | -0.3 | -3.3 | Γ_1 |
| Γ_1 | -10.7 | -10.7 | -11.6 | -9.8 | -9.8 | -11.0 | -9.5 | -9.6 | -10.8 | -11.1 | -11.3 | -12.2 | -11.2 | -11.4 | -11.9 | Γ_1 |
| X_2 | 10.9 | 11.0 | 11.3 | 10.4 | 10.5 | 10.7 | 10.5 | 10.5 | 10.8 | 12.3 | 12.7 | 12.9 | 13.1 | 13.7 | 13.7 | X_2 |
| $X_{4'}$ | 9.1 | 8.7 | 8.5 | 8.7 | 8.5 | 8.2 | 8.5 | 8.3 | 7.8 | 8.3 | 8.4 | 8.5 | 8.2 | 8.5 | 8.8 | $X_{4'}$ |
| $X_{5'}$ | 7.2 | 7.0 | 7.0 | 7.3 | 7.2 | 7.0 | 7.4 | 7.4 | 6.7 | 8.2 | 8.6 | 7.8 | 8.8 | 9.3 | 8.2 | $X_{5'}$ |
| X_3 | 3.5 | 4.2 | 4.3 | 3.6 | 4.4 | 4.5 | 3.8 | 4.6 | 4.9 | 4.9 | 6.1 | 6.1 | 5.5 | 6.9 | 6.7 | X_3 |
| $X_{5'}$ | -2.0 | -1.8 | -1.8 | -1.7 | -1.5 | -1.5 | -1.5 | -1.3 | -1.3 | -1.3 | -1.1 | -1.1 | -1.2 | -1.0 | -1.0 | $X_{5'}$ |
| $X_{4'}$ | -4.2 | -3.8 | -3.8 | -3.6 | -3.2 | -3.2 | -3.3 | -2.9 | -2.9 | -3.1 | -2.6 | -2.7 | -3.0 | -2.4 | -2.6 | $X_{4'}$ |
| X_1 | -4.8 | -5.0 | -5.7 | -3.2 | -3.1 | -4.2 | -2.7 | -2.5 | -5.6 | -1.9 | -1.1 | -4.5 | -1.0 | -0.2 | -3.7 | X_1 |
| X_1 | -8.2 | -8.4 | -9.8 | -8.0 | -8.3 | -9.8 | -7.9 | -8.3 | -9.6 | -10.1 | -10.6 | -11.4 | -10.2 | -10.7 | -11.1 | X_1 |
| L_1 | 10.5 | 10.8 | 10.7 | 9.5 | 10.0 | 9.9 | 9.3 | 9.8 | 9.9 | 10.0 | 10.9 | 11.1 | 10.6 | 11.7 | 11.7 | L_1 |
| $L_{3'}$ | 1.7 | 2.0 | 2.0 | 2.4 | 2.8 | 2.8 | 2.7 | 3.2 | 3.2 | 4.1 | 4.9 | 4.5 | 4.9 | 5.9 | 5.1 | $L_{3'}$ |
| $L_{2'}$ | 2.4 | 2.6 | 2.2 | 2.3 | 2.7 | 2.2 | 2.4 | 2.8 | 1.7 | 2.5 | 3.4 | 2.5 | 2.9 | 4.0 | 2.9 | $L_{2'}$ |
| L_1 | 1.9 | 1.8 | 1.7 | 2.9 | 2.8 | 2.3 | 3.2 | 3.1 | 1.5 | 4.0 | 4.1 | 2.2 | 4.7 | 4.7 | 2.7 | L_1 |
| L_3 | 0.4 | 0.4 | 0.4 | 0.2 | 0.1 | 0.2 | 0.1 | 0.1 | 0.2 | 0.0 | 0.0 | 0.2 | 0.0 | 0.0 | 0.3 | L_3 |
| L_1 | -7.2 | -7.0 | -7.4 | -5.6 | -5.3 | -6.0 | -5.2 | -4.8 | -6.8 | -4.8 | -4.1 | -6.1 | -4.4 | -3.7 | -5.6 | L_1 |
| $L_{2'}$ | -8.5 | -8.7 | -10.0 | -8.3 | -8.6 | -10.0 | -8.2 | -8.5 | -9.6 | -10.2 | -10.7 | -11.4 | -10.3 | -10.8 | -11.2 | $L_{2'}$ |

Now for a few words about our notation. It is convenient to use the symbol E (REL) to denote the full relativistic energy level scheme, as given by a relativistic band calculation; and the symbol E^* (REL) to denote the closely related scheme in which spin-orbit split levels in E (REL) are represented by their weighted means. The ordinary non-relativistic energy level scheme E (NREL) and the *reduced* relativistic scheme E^* (REL) are both expressed in single group notation, while the E (REL) scheme is expressed in double group notation [23]. Apart from exceptional cases where nearby levels in the E (REL) scheme are strongly coupled by the spin-orbit interaction, the passage from E (REL) to E^* (REL) is straightforward.

Some of the E (REL) solutions based on Slater exchange are listed in table II. The spin-orbit splittings ΔE (SO) are also shown here for convenience. The reduced scheme E^* (REL) based on Slater exchange is displayed in table I. The E (REL) and E^* (REL) schemes based on Kohn-Sham exchange are not shown because they bear the same relation to the Slater-type E (REL) and E^* (REL) schemes that the corresponding E (NREL) schemes displayed in table I do to one another. Moreover, both treatments of exchange lead to spin-orbit splittings which usually agree to within a few hundredths of an eV.

To avoid possible complications with switched band edges at L (See section VI) the zero of energy

TABLE II

Electronic energy levels for GeTe, SnTe, PbTe, PbSe, and PbS, based on relativistic OPW band calculations (Slater exchange). All entries are in eV.

| Atomic character | | Single group | Double group | GeTe | | SnTe | | PbTe | | PbSe | | PbS | |
|------------------|-----|----------------|--------------|-----------------|-----------|-----------------|-----------|-----------------|-----------|-----------------|-----------|-----------------|-----------|
| IV | VI | Level | Level | ΔE (SO) | E (REL) | ΔE (SO) | E (REL) | ΔE (SO) | E (REL) | ΔE (SO) | E (REL) | ΔE (SO) | E (REL) |
| d | d | Γ_{12} | Γ_8^+ | | 8.73 | | 8.41 | | 8.58 | | 10.50 | | 11.34 |
| d | d | $\Gamma_{25'}$ | Γ_7^+ | 0.03 | 6.83 | 0.04 | 6.71 | 0.07 | 6.95 | 0.07 | 8.63 | 0.05 | 9.45 |
| | | | Γ_8^+ | | 6.80 | | 6.67 | | 6.88 | | 8.56 | | 9.40 |
| p | (p) | Γ_{15} | Γ_8^- | 0.56 | 5.18 | 0.80 | 5.64 | 2.08 | 5.93 | 2.26 | 7.83 | 2.34 | 8.71 |
| | | | Γ_6^- | | 4.62 | | 4.84 | | 3.85 | | 5.57 | | 6.37 |
| (p) | p | Γ_{15} | Γ_8^- | 0.71 | 0.00 | 0.81 | 0.00 | 1.03 | 0.00 | 0.55 | 0.00 | 0.26 | 0.00 |
| | | | Γ_6^- | | — 0.71 | | — 0.81 | | — 1.03 | | — 0.55 | | — 0.26 |
| s | s | Γ_1 | Γ_6^+ | | — 3.83 | | — 3.05 | | — 4.54 | | — 4.09 | | — 3.36 |
| (s) | s | Γ_1 | Γ_6^+ | | — 11.87 | | — 11.28 | | — 11.14 | | — 12.38 | | — 12.02 |
| d | d | X_2 | X_7^+ | | 11.02 | | 10.47 | | 10.51 | | 12.68 | | 13.58 |
| p | p | X_4 | X_6^- | | 8.31 | | 7.91 | | 7.48 | | 8.28 | | 8.73 |
| p | p | $X_{5'}$ | X_7^- | 0.52 | 6.98 | 0.67 | 7.08 | 1.51 | 7.09 | 1.60 | 8.44 | 1.68 | 8.97 |
| | | | X_6^- | | 6.46 | | 6.41 | | 5.58 | | 6.84 | | 7.29 |
| d | d | X_3 | X_7^+ | | 4.07 | | 4.23 | | 4.54 | | 5.91 | | 6.61 |
| p | p | $X_{5'}$ | X_7^- | 0.35 | — 1.86 | 0.43 | — 1.52 | 0.67 | — 1.32 | 0.42 | — 1.10 | 0.25 | — 0.92 |
| | | | X_6^- | | — 2.21 | | — 1.95 | | — 1.99 | | — 1.52 | | — 1.17 |
| p | p | X_4 | X_6^- | | — 4.05 | | — 3.45 | | — 3.22 | | — 2.86 | | — 2.67 |
| s | (s) | X_1 | X_6^+ | | — 5.96 | | — 4.48 | | — 5.91 | | — 4.71 | | — 3.84 |
| (s) | s | X_1 | X_6^+ | | — 10.02 | | — 10.04 | | — 9.90 | | — 11.57 | | — 11.21 |
| (s, d) | p | L_1 | L_6^+ | | 10.51 | | 9.69 | | 9.57 | | 10.90 | | 11.65 |
| p | (d) | $L_{3'}$ | L_{45}^+ | 0.14 | 1.87 | 0.23 | 2.67 | 0.50 | 3.07 | 0.83 | 4.73 | 0.91 | 5.48 |
| | | | L_6^- | | 1.73 | | 2.44 | | 2.57 | | 3.90 | | 4.57 |
| (p) | s | $L_{2'}$ | L_6^- | | 1.96 | | 1.96 | | 1.37 | | 2.36 | | 2.81 |
| s | p | L_1 | L_6^+ | | 1.43 | | 1.99 | | 1.12 | | 2.03 | | 2.57 |
| (d) | p | L_3 | L_{45}^+ | 0.60 | 0.44 | 0.55 | 0.21 | 0.58 | 0.17 | 0.22 | 0.17 | 0.04 | 0.25 |
| | | | L_6^+ | | — 0.16 | | — 0.34 | | — 0.41 | | — 0.05 | | — 0.21 |
| s | (p) | L_1 | L_6^+ | | — 7.65 | | — 6.24 | | — 7.10 | | — 6.24 | | — 5.64 |
| (p) | s | $L_{2'}$ | L_6^- | | — 10.26 | | — 10.22 | | — 9.98 | | — 11.58 | | — 11.26 |

in tables I and II has been placed at the highest valence band level at the zone center. Since the zero of energy in table I occurs at a Γ_{15} level, and in table II at a Γ_8^- level, corresponding non-degenerate levels in these two tables are displaced from one another by 1/3 of the spin-orbit splitting of the Γ_{15} level.

IV. Relativistic corrections in retrospect. — Since we have analogous E (NREL), E (REL), and E^* (REL) solutions at our disposal, we can define the relativistic corrections ΔE (REL) as follows : ΔE (REL) = E^* (REL) — E (NREL). By comparing the relativistic corrections thus defined with the estimates given by perturbation theory [6-9, 27] we can determine how accurate these estimates really are. In the case of the lead salts, we find that the perturbation estimates are often in error by as much as 0.2 eV for interband energies that are affected only moderately by the inclusion of relativistic effects, and by as much as 0.4 eV for strongly affected interband energies. Considering that some of the relativistic corrections are as large as 3 eV for these materials, perturbation theory is seen to give reasonably good estimates. However, if one is striving for a mathematical accuracy approaching 0.1 eV, the perturbation approach is clearly deficient.

Part of the difficulty with the perturbation approach stems from the approximate nature of the relativistic correction terms that appear in first-order perturbation theory [6-9, 27]. Another difficulty is that the perturbation approach neglects the change in self-consistent atomic potentials associated with the inclusion of relativistic terms [28]. In spite of these shortcomings, however, the perturbation approach usually gives reasonable results, not only for the relativistic corrections ΔE (REL), but also for the spin-orbit splittings ΔE (SO).

In any event, it is clear that relativistic and spin-orbit coupling effects must be taken into account if realistic energy band pictures are to be determined.

V. Preliminary energy band pictures for the IV-VI compounds. — Although it is possible in principle to map out the band structure throughout the reduced zone by carrying out first-principles band calculations at a sufficiently large number of points, it is more economical (and nearly as satisfactory) to carry out such calculations only at a few key points, and then to extend the solutions into the remainder of the zone with the aid of a parametric interpolation scheme [18-20].

Using a modified pseudopotential interpolation scheme similar to that described in earlier publica-

tions [18-20] interpolated energy band pictures of the E^* (REL) type have been obtained for GeTe, SnTe, PbTe, PbSe, and PbS. These band pictures were adjusted (by least-squares) to the three highest valence and the three lowest conduction band levels of the E^* (REL) type at Γ , X , L , and Σ ($\frac{1}{2}$ $\frac{1}{2}$ 0). In some cases, additional E^* (REL) levels at A ($\frac{1}{2}$ 0 0) and W were also employed. This interpolation scheme, which is based on a local pseudopotential and a kinetic energy term containing an adjustable effective mass parameter, is able to reproduce the E^* (REL) levels reasonably well over a 10 eV range extending roughly 5 eV below and 5 eV above the direct band gap at L . Beyond this range (and even on the fringes of this range), the interpolation scheme breaks down, failing to reproduce the first-principles E^* (REL) levels with any degree of accuracy.

The interpolated band pictures (for the Slater-type solutions) were then improved in two ways. In the first place, we drew free-hand sketches of the energy bands in some of the regions where the interpolation scheme was defective. In the second place, the spin-orbit splitting was incorporated into the final pictures so that we would match the E (REL) levels at the points where these levels had been calculated from first principles. Of course, this involved estimating the spin-orbit splitting at intermediate points in the zone, but this is not too difficult to do if one is content with an accuracy of a few tenths of an eV.

The preliminary energy band pictures shown in figs. 1 through 5 are based on the first-principles E (REL) levels at key points in the zone, and on interpolation and spin-orbit splitting estimates elsewhere in the zone. We believe that these pictures represent the first-principles E (REL) levels throughout the zone to within a few tenths of an eV over an energy range of about 10 eV.

In order to obtain more accurate renditions of our E (REL) solutions throughout the zone, it will be necessary to use a more sophisticated (possibly a non-local, energy-dependent) interpolation scheme which is valid over a wider energy range, and includes a simulated spin-orbit interaction term [29]. Such a scheme could be fitted directly to the E (REL) levels at key points in the zone, thus avoiding the intermediate step of an adjustment to the reduced E^* (REL) levels. Of course, we could also obtain first-principles E (REL) levels at a few additional points in the zone to improve the first-principles sample.

At this writing we have nearly completed the development of an improved interpolation scheme of the type just described, but until this scheme becomes

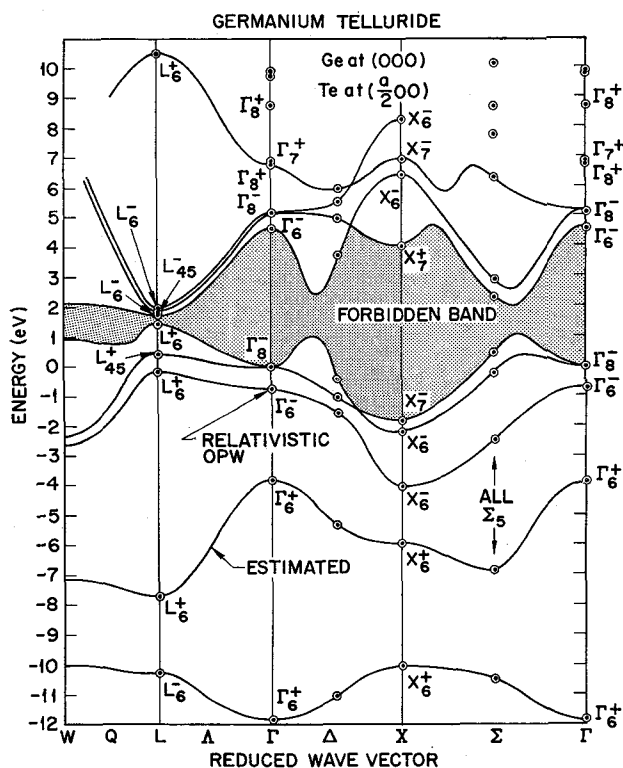
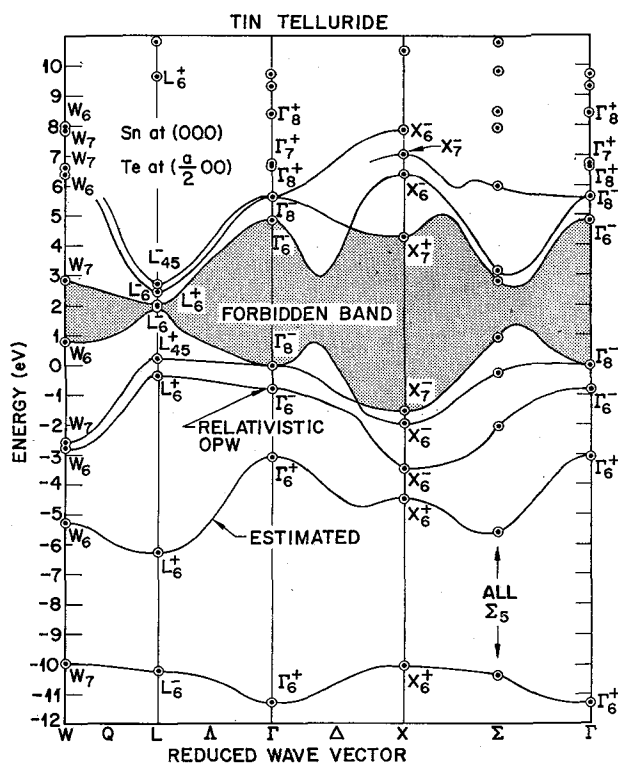


FIG. 1. — Energy band structure of GeTe (Slater exchange).

operational, we will have to be content with the preliminary band pictures shown in figs. 1 through 5.

It is clear from these figures that the energy level schemes of GeTe, SnTe, PbTe, PbSe, and PbS have a great deal in common, though there are obviously systematic differences from crystal to crystal arising from chemical shifts, differences in lattice constant, and differences in the magnitude of the spin-orbit splitting. (Relativistic shifts are here included in the catch-all expression «chemical shifts».) But even allowing for these systematic differences, it is evident that over an energy range of about 20 eV, most of the valence and conduction band levels at key points in the zone occur in nearly the same general order.

To dramatize this point, we present a composite view of the E (REL) levels at Γ , X , L , and Σ ($\frac{1}{2}$ $\frac{1}{2}$ 0) for the five IV-VI compounds in fig. 6. It is interesting to note that there is more regularity in the PbS-PbSe-PbTe sequence than in the GeTe-SnTe-PbTe sequence. Since the chemical shifts and the spin-orbit splittings vary in a regular manner in both sequences, the contrast just noted might arise from lattice constant effects. Indeed, if one compares the lattice constant differences in the PbS-PbSe-PbTe sequence (cf. table III) with the corresponding diffe-

FIG. 2. — Energy band structure of SnTe (Slater exchange). Note that our symmetry designations agree with those of Lin and Kleinman [10] at Γ , X , and L but not at W .

rences in analogous sequences such as HgS-HgSe-HgTe, CdS-CdSe-CdTe, and ZnS-ZnSe-ZnTe, one finds a remarkable degree of similarity; while if one compares GeTe-SnTe-PbTe with an analogue such as ZnTe-CdTe-HgTe (or even ZnSe-CdSe-HgSe or ZnS-CdS-HgS) one finds a definite lack of similarity. The change in lattice constant in going from GeTe to SnTe is about 2.5 times as large as that in going from SnTe to PbTe, while in the other sequences, the change in going from ZnX to CdX is an order of magnitude larger than that in going from CdX to HgX, where $X = \text{Te, Se, or S}$. For all of these sequences to be similar, we would require the lattice constants of SnTe and PbTe to be closer together than they actually are (cf. table III). Presumably, the irregularity of the energy levels in the GeTe-SnTe-PbTe sequence could be removed (theoretically) by increasing the lattice constant of SnTe and/or decreasing the lattice constant of PbTe. If these arguments are correct, then the energy levels of normal GeTe, normal SnTe, and PbTe under extreme pressure should show a higher degree of regularity than is evident in figure 6.

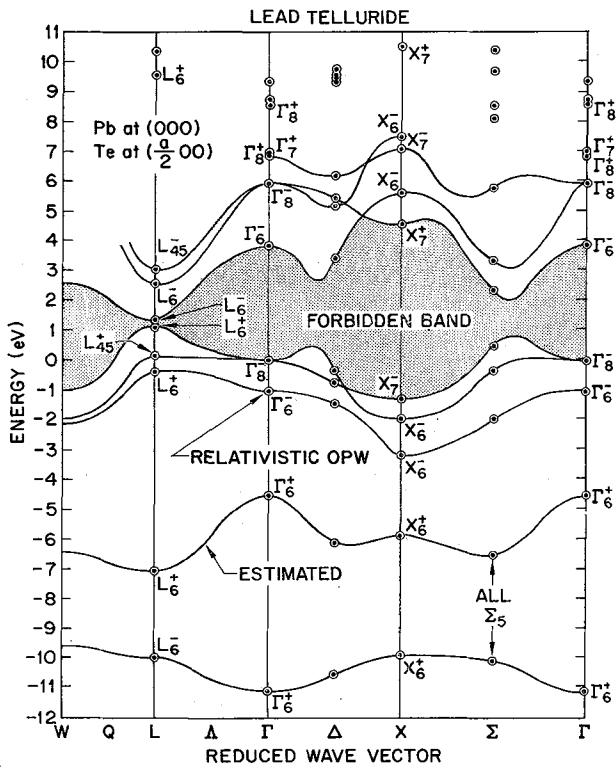


FIG. 3. — Energy band structure of PbTe (Slater exchange).

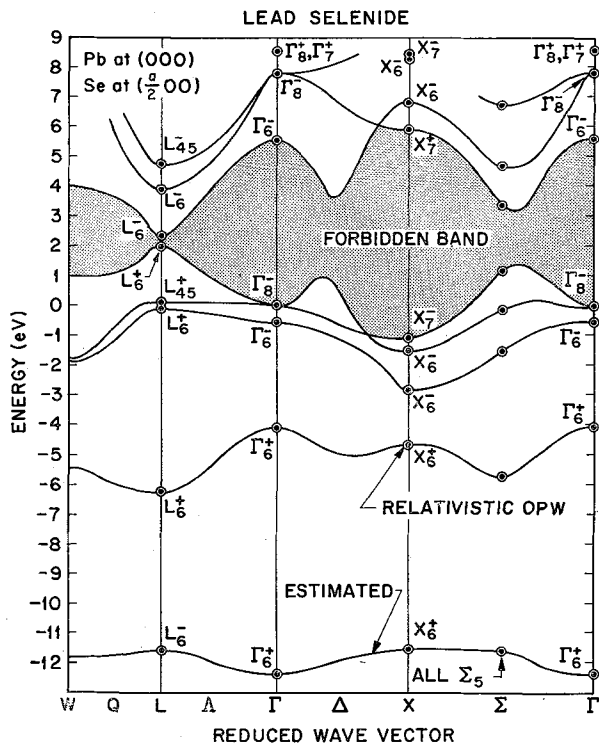


FIG. 4. — Energy band structure of PbSe (Slater exchange).

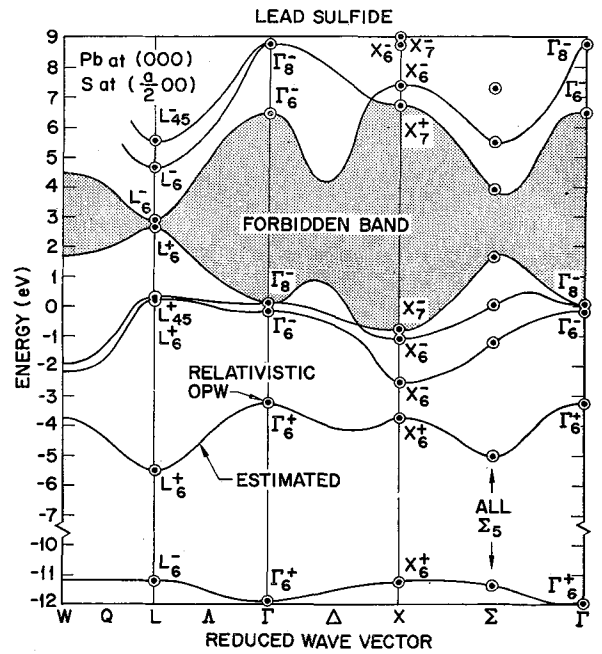


FIG. 5. — Energy band structure of PbS (Slater exchange).

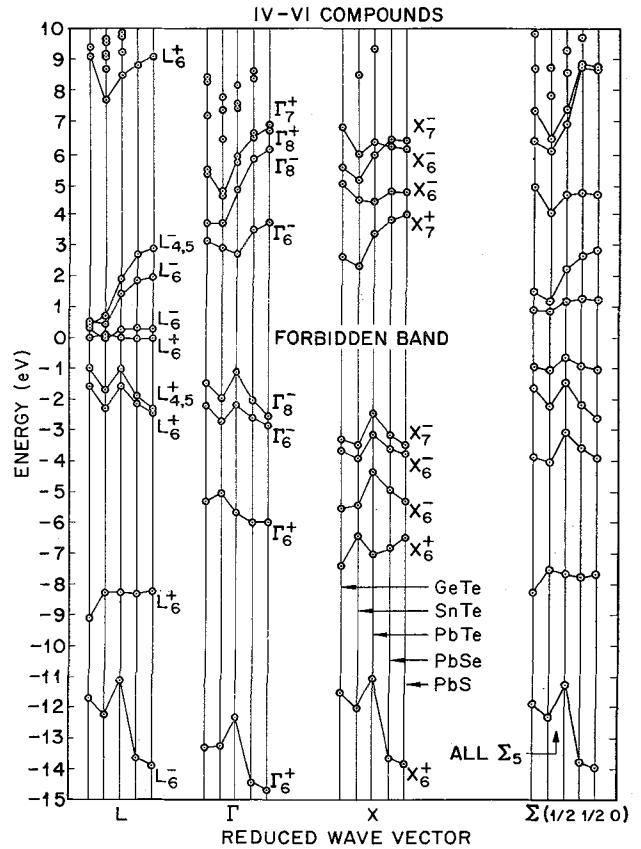


FIG. 6. — Composite view of electronic energy levels of GeTe, SnTe, PbTe, PbSe, and PbS at key points in the reduced zone (Slater exchange).

TABLE III

Calculated energy levels for uppermost core d bands ^(a) and lattice constants used in the band calculations ^(b)

| | GeTe | SnTe | PbTe | PbSe | PbS |
|------------------|-----------------------------|-----------------------------|-----------------------------|-----------------------------|-----------------------------|
| Cation d band | Ge 3d — 27.03 — 27.67 | Sn 4d — 21.03 — 22.15 | Pb 5d — 14.98 — 17.74 | Pb 5d — 13.53 — 16.28 | Pb 5d — 12.62 — 15.37 |
| Anion d band | Te 4d — 37.94 — 39.50 | Te 4d — 38.34 — 39.91 | Te 4d — 38.47 — 40.04 | Se 3d — 52.60 — 53.57 | |
| Lattice constant | 11.357 | 11.958 | 12.196 | 11.573 | 11.218 |

^(a) Energy eigenvalues (in electron volts), as given by relativistic OPW band calculations based on Slater exchange. The spin doublets shown here belong to the same E (REL) scheme as the valence and conduction band levels displayed in table II. The zero of energy here is defined by the highest valence band level at the zone center, L_6^- (consistent with table II).

^(b) All lattice constants are expressed in Bohr units. The value for GeTe corresponds to the high temperature rock-salt phase (Ge-rich boundary of phase diagram at 460 °C): see PEARSON (W. B.), *A Handbook of Lattice Spacings and Structures of Metals and Alloys* (Pergamon Press, New York, 1958), p. 680. The value for SnTe is adapted from MAZELSKY (R.), LUBELL (M. S.), and KRAMER (W. E.), *J. Chem. Phys.*, 1962, 37, 45. The values for PbTe, PbSe, and PbS are adapted from WYCKOFF (R. W. G.), *Crystal Structures* (Interscience Publishers, New York, 1963), Second Edition, Vol. 1, p. 89.

VI. Comments on the experimental situation. —

Before comparing our theoretical results with experiment, let us recapitulate some of the current ideas about the electronic structure of PbTe and related crystals. It is widely believed [1-10] that the principal band edges in PbS, PbSe, and PbTe occur at the L point in the reduced zone, and that the symmetry classification of these band edges is the same in all three crystals: valence band edge = L_6^+ and conduction band edge = L_6^- in double group notation. This view is consistent with the fact that the temperature and pressure dependence of the direct band gaps in these three crystals is nearly the same. Various transport measurements suggest the presence of a subsidiary valence band edge just below the principal valence band edge in PbTe (and possibly also in PbSe and PbS), but the detailed nature of this subsidiary edge is uncertain.

According to a recently proposed energy band model for the $Pb_xSn_{1-x}Te$ alloy system [30], the valence and conduction band edges remain at the L points over the entire composition range, but L_6^+ and L_6^- switch roles at an intermediate composition. In order to account for the fact that the band gap becomes

smaller if Sn is added to Pb-rich alloys, and also if Pb is added to Sn-rich alloys, this model regards the L_6^+ and L_6^- levels as coming together and then crossing, as one traverses the alloy system in either direction. Because of the crossover, the valence band edge in SnTe (and in Sn-rich alloys) is defined by L_6^- , and the conduction band edge by L_6^+ .

Just as the band gaps of PbTe, PbSe, and PbS all increase with increasing temperature, so the band gaps of SnTe and GeTe both decrease with increasing temperature [31]. This contrast in temperature dependence suggests (but does not prove conclusively) that the principal band edges in GeTe are more nearly akin to those in SnTe than to those in PbTe. That is to say, if the direct band gap in GeTe occurs at points related to L (recall that GeTe is actually rhombohedral rather than cubic at room temperature and below), then the valence and conduction band edges will be derived from L_6^- and L_6^+ levels, respectively.

There is also some evidence for subsidiary valence band edges in SnTe and GeTe [32] but the zone location and symmetry classification of these edges remain open questions, though there is some theoretical support for maxima along the Σ axes in SnTe [11].

The optical reflectivity measurements of Cardona and Greenaway [33] the photoemission measurements of Spicer and his co-workers [34] and the electroreflectivity measurements of Aspnes and Cardona [35, 36] and of Seraphin [37] all provide important potential sources of information regarding the overall band structure of various IV-VI compounds. In fact, the pioneering empirical pseudopotential band models for the lead salts [10] were based in large measure on a plausible (though not necessarily unique) interpretation of Cardona and Greenaway's reflectivity spectra. Although it is very easy to interpret most of these measurements in the spirit of an educated guessing game, it is becoming increasingly evident from detailed examinations of better-understood crystals — such as tetrahedrally-bonded semiconductors [14-21] — that mere guesswork often falls far off the mark, and that tentative (or even categorical) assignments of spectral structure should be treated with the greatest caution. One of the objectives of the present study, of course, is to provide improved energy band models which hopefully will reduce the uncertainty of current theoretical interpretations of experimental spectra.

VII. Comments on the theoretical situation. — As we have indicated in a recent series of papers [14-21] our approach to band structure calculations involves two essential steps. In the first step, we carry out a

first-principles band calculation and thereby obtain a provisional energy band picture. In the second step, we introduce an empirical correction which brings the theoretical band picture into exact (or close) agreement with the best established experimental features. In practice, this amounts to changing a few features of the trial crystal potential so that a corresponding number of interband energy separations are in accord with experiment. Treating this change in the trial crystal potential as a perturbation (which it normally is), we then recalculate the entire band structure, and thereby obtain a modified band picture which hopefully agrees better with experiment not only in the fitted regions, but in the unfitted regions as well.

In the case of tetrahedrally-bonded semiconducting compounds [17-21] we have usually been able to make substantial improvements in our first-principles solutions, where such improvements prove necessary, by using a three-parameter empirical correction scheme. Two of these parameters are used to modify the effective crystal potential in the cation and anion core regions, and the third to raise or lower the potential in the interstitial region relative to the core regions.

In order to make similar progress in the present study, it is necessary to know three or more interband energy separations (per crystal) with a high degree of certainty. Reviewing the experimental information included in table IV, we find that apart from the direct band gaps, there are hardly any other transition energies that can be assigned to specific interband transitions (at precise positions in the zone) with an accuracy of the order of 0.1 eV. It should be borne in mind that the reflectivity peaks are associated with interband transitions belonging to extensive regions of the reduced zone: such associations usually provide only a rough measure of the key interband transitions which characterize these regions. Although the electroreflectivity (ER) peaks can usually be measured quite accurately, the identification of these peaks is often ambiguous.

As can be seen from table I, where the E (NREL) solutions for the Slater and Kohn-Sham exchange models are compared, the Kohn-Sham model usually leads to smaller energy separations between the valence and the conduction bands. Since both of these models are based on a variety of physical approximations, we should not expect either model to lead to a band structure which agrees exactly with experiment. In fact, the difference between the Slater and Kohn-Sham solutions provides a realistic measure of the uncertainty in the calculated band structure

associated with the uncertainty in present-day treatments of exchange (and correlation) effects. Since we have found in earlier studies of II-VI compounds [18-20] that the Slater model gives results in closer agreement with experiment than the Kohn-Sham model, we would be inclined to favor the Slater model in the present study of IV-VI compounds. At the same time, we have found the Kohn-Sham model to be superior in some respects in applications to column IV semiconductors and III-V compounds [20-21]. Hence we cannot dismiss the Kohn-Sham model, especially in the case of GeTe and SnTe.

In practice, we find that the Slater solutions give a better account of the experimental situation for the IV-VI compounds than the Kohn-Sham solutions do. It is for this reason that we have concentrated on the Slater solutions in table II and in figures 1 through 6.

In the next section, we will relate the first-principles E (REL) solutions to experiment. By doing so, we will be able to check the adequacy of these solutions and at the same time pave the way for subsequent empirical refinements [13].

VIII. Comparison between theory and experiment. —

The Slater (and also the Kohn-Sham) E (REL) solutions place the principal valence and conduction band edges at L in all five crystals, in accord with experiment (at least for SnTe, PbTe, PbSe, and PbS; the experimental situation in GeTe is uncertain). In the case of the lead salts, the Slater model leads to the correct ordering of L_6^- and L_6^+ in the neighborhood of the band gap, as well as to remarkably accurate values for the band gaps themselves. Because the three conduction bands have moved down relative to the valence bands in the Kohn-Sham model, the ordering of L_6^- and L_6^+ is incorrectly given by this model, and the band gap differs from experiment by several tenths of an eV.

In the case of SnTe, both exchange models place L_6^+ above L_6^- , in accord with experiment [30]; the experimental band gap, 0.2 eV [30-32] falls midway between the Slater and Kohn-Sham values ($L_6^+ - L_6^- = 0.03$ and 0.46 eV, respectively).

In the present study, GeTe is assumed to have the rock-salt structure, and a lattice constant corresponding to an elevated temperature (cf. table III). However, most of the experimental evidence refers to the rhombohedral form of GeTe [38] at room temperature and below [31, 32]. In particular, the band gap of rhombohedral GeTe at room temperature is about 0.1 eV [32]. Since the experimental band gap decreases with increasing temperature,

we should compare our theoretical band gaps with a « high temperature » band gap of about 0 eV. Our Kohn-Sham band gap ($L_6^- - L_6^+$) is 0.02 eV, while the corresponding Slater value is 0.30 eV. If the difference between the rhombohedral and rock-salt crystal structures makes no appreciable difference in the magnitude of the direct band gap, then the Kohn-Sham model is in better agreement with experiment than the Slater model. However, if the crystal structure difference could change the band gap by a few tenths of an eV, both models must be considered within striking distance of experiment. (We plan to carry out relativistic OPW band calculations for rhombohedral GeTe using the room temperature lattice parameters [38] so that we can come closer to the actual experimental situation.)

The direct band gap at L (between bands 5 and 6) defines an M_0 critical point: the surfaces of constant energy separation are ellipsoidal in the vicinity of L . The well-defined valence band maxima and conduction band minima along the Δ and Σ axes in figures 1 through 5 are not necessarily subsidiary band edges, since the valence band energy may increase (and the conduction band energy may decrease) as one moves away from these axes in one or more perpendicular direction. Our solutions suggest that the highest valence band maxima and the lowest conduction band minima along the Δ and Σ axes are more likely to be saddle points than absolute extrema. Moreover, the minimum energy separations along the Δ and Σ axes define M_2 and M_1 critical points, since the surfaces of constant energy separation are hyperbolic in these neighborhoods. In the future, we will refer to these as the Δ and Σ saddle points.

Reflectivity Spectra. Cardona and Greenaway [33] (hereafter CG) have measured the reflectivity spectra of GeTe, SnTe, PbTe, PbSe, PbS, and related materials. They have arranged corresponding reflectivity peaks and shoulders into families and labeled these E_1 to E_6 . The experimental results of CG are very useful because they contain many important clues regarding the overall band structure of these materials. In the following discussion, we will offer an interpretation of these results which is based partly on the correlation with our theoretical energy level separations (cf. table IV), and partly on the outcome of some preliminary optical spectrum calculations which we have carried out for SnTe (see also Lin *et al.* [11] for an analysis of the reflectivity spectrum of SnTe).

It is by now widely recognized that reflectivity peaks are associated with electronic transitions between pairs of bands which remain nearly parallel

to one another over a significant fraction of the reduced zone. In simple cases it is convenient to discuss these regions of nearly constant energy separation in terms of related critical points; in more complex cases such a discussion may not be particularly illuminating. In the present application, it is important to bear in mind that large regions of nearly constant energy separation may be associated with Σ and Δ saddle points, as well as with such symmetry points as Γ , X , L , and W .

As an illustration, let us consider band 5 \rightarrow band 6 transitions in SnTe. Although it is not evident from figure 2, the interband separation is nearly constant in a region which starts at the Σ saddle point and extends in the general direction of L , and in another region which starts at the Δ saddle point and extends in the direction of the Δ axis.

The E_1 structure (absorption shoulder in SnTe; weak reflectivity peak in PbTe, PbSe, and PbS) appears to arise primarily from band 5 \rightarrow band 6 transitions in a region close to the Σ saddle point which extends toward L . In the lead salts, we would also expect significant contributions from band 5 \rightarrow band 7 transitions in a region close to L which extends toward Σ (cf. table IV). In GeTe, the absorption threshold at about 0.6 eV (as measured in transmission by Aspnes and Cardona [36]) may be associated with band 5 \rightarrow band 7 and band 5 \rightarrow band 8 transitions in the neighborhood of the L points, or even with band 5 \rightarrow band 6 transitions in the vicinity of the Σ saddle point. In any event, the observed absorption threshold should lie slightly above the related minimum band gap, because of the high carrier concentration (Burstein effect).

The E_2 structure (main reflectivity peak) appears to arise from various types of transitions. In SnTe, PbTe, PbSe, and PbS, the principal contributions appear to come from band 5 \rightarrow band 6 transitions in the vicinity of the Δ saddle point, and from band 4 \rightarrow band 6 and band 5 \rightarrow band 7 transitions in the neighborhood of the Σ saddle point. In GeTe, band 3 \rightarrow bands 7 and 8 transitions near L may play a role in addition to those just mentioned (cf. table IV).

The E_3 structure (shoulder or weak reflectivity peak) also appears to arise from more than one type of transition. In SnTe, PbTe, PbSe, and PbS, the principal contribution appears to come from band 4 \rightarrow band 7 transitions near the Σ saddle point; in some of these materials there may also be significant contributions from bands 3 and 4 \rightarrow band 6 transitions near the Δ saddle point, and even from bands 3 and 4 \rightarrow band 8 transitions near L . In GeTe,

TABLE IV — Comparison of theoretical and experimental interband transition energies ^(a). All entries are in eV

| Transition energy ^(b) | GeTe | SnTe | PbTe | PbSe | PbS |
|---|---------------------|---------------------|--------------------------|--------------------------------------|---|
| | <i>E</i> (REL) EXPT | <i>E</i> (REL) EXPT | <i>E</i> (REL) EXPT | <i>E</i> (REL) EXPT | <i>E</i> (REL) EXPT |
| <i>E</i> ₀ (band gap) | 0.1 ^(c) | 0.2 ^(c) | 0.32 ^(d) | 0.27 ^(d) | 0.42 ^(d) |
| <i>L</i> ₆ ⁻ (6) - <i>L</i> ₆ ⁺ (5) | 0.30 (0.02) | | 0.25 (-0.17) | 0.33 (-0.44) | 0.24 (-0.54) |
| <i>L</i> ₆ ⁺ (6) - <i>L</i> ₆ ⁻ (5) | | 0.03 (0.46) | | | |
| <i>E</i> ₁ (reflectivity) ^(e) | | 0.9-1.0 | 1.24 | 1.54 | 1.83 |
| $\Sigma_5(6) - \Sigma_5(5)$ | ~ 0.9 | ~ 1.2 | ~ 1.2 (1.2) | ~ 1.8 (1.53) | ~ 2.0 (1.85) |
| <i>L</i> ₆ ⁻ (7) - <i>L</i> ₆ ⁺ (5) | 0.4 | 0.5 ^(f) | 1.5 (1.6) | 1.9 (1.78) | 2.0 (1.98) |
| <i>L</i> ₆ ⁻ (6) - <i>L</i> ₄₅ ⁺ (4) | 1.3 | 1.8 ^(f) | 1.2 | 2.2 (2.05) | 2.6 |
| <i>L</i> ₆ ⁻ (6) - <i>L</i> ₆ ⁺ (3) | 1.9 | 2.3 ^(f) | 1.8 | 2.4 | 2.6 |
| <i>L</i> ₄₅ ⁻ (8) - <i>L</i> ₆ ⁺ (5) | 0.5 | 0.7 ^(f) | 2.0 | 2.7 | 2.9 |
| <i>E</i> ₂ (reflectivity) ^(e) | 1.98 | 2.07 | 2.45 | 3.12 | 3.67 |
| $\Delta_6(6) - \Delta_6(5)$ | ~ 1.4 | ~ 2.2 | ~ 2.2 | ~ 2.8 | ~ 3.4 |
| $\Sigma_5(6) - \Sigma_5(4)$ | ~ 1.6 | ~ 2.5 | ~ 2.0 | ~ 3.2 | ~ 3.5 |
| $\Sigma_5(7) - \Sigma_5(5)$ | ~ 1.5 | ~ 1.7 | ~ 2.3 | ~ 3.2 | ~ 3.7 |
| <i>L</i> ₆ ⁻ (7) - <i>L</i> ₄₅ ⁺ (4) | 1.4 | 2.3 | 2.4 | 3.8 | 4.4 |
| <i>L</i> ₆ ⁻ (7) - <i>L</i> ₆ ⁺ (3) | 2.0 | 2.8 | 3.0 | 4.0 | 4.4 |
| <i>L</i> ₄₅ ⁻ (8) - <i>L</i> ₄₅ ⁺ (4) | 1.5 | 2.5 | 2.9 | 4.6 | 5.3 |
| <i>L</i> ₄₅ ⁻ (8) - <i>L</i> ₆ ⁺ (3) | 2.1 | 3.0 | 3.5 | 4.8 | 5.3 |
| <i>E</i> ₃ (reflectivity) ^(e) | 3.2 | 3.2 | 3.5 | 4.5 | 5.3 |
| $\Sigma_5(7) - \Sigma_5(4)$ | ~ 2.2 | ~ 3.0 | ~ 3.1 | ~ 4.6 | ~ 5.2 |
| $\Delta_6(6) - \Delta_7(4)$ | ~ 3.0 | ~ 3.5 | ~ 3.1 | ~ 4.2 | ~ 4.4 |
| $\Delta_6(6) - \Delta_6(3)$ | ~ 3.6 | ~ 4.2 | ~ 3.9 | ~ 4.6 | ~ 4.6 |
| <i>E</i> ₄ (reflectivity) ^(e) | 6.2 ^(g) | 6.1 | 6.3 | 7.1 | 8.1 |
| <i>X</i> ₇ ⁺ (6) - <i>X</i> ₇ ⁻ (5) | 5.9 | 5.8 | 5.9 | 7.0 | 7.5 |
| <i>X</i> ₇ ⁺ (6) - <i>X</i> ₆ ⁻ (4) | 6.3 | 6.2 | 6.5 | 7.4 | 7.8 |
| <i>E</i> ₅ (reflectivity) ^(e) | 7.8 ^(g) | 7.4 | 7.8 | 9.1 | 9.8 |
| $\Gamma_7^+(11) - \Gamma_6^-(3)$ | 7.5 | 7.5 | 7.9 | 9.1 | 9.7 |
| $\Gamma_8^+(9,10) - \Gamma_6^-(3)$ | 7.5 | 7.5 | 8.0 | 9.2 | 9.7 |
| $\Gamma_6^-(6) - \Gamma_6^+(2)$ | 8.5 | 7.9 | 8.4 | 9.7 | 9.7 |
| <i>X</i> ₇ ⁺ (6) - <i>X</i> ₆ ⁻ (3) | 8.1 | 7.7 | 7.8 | 8.8 | 9.3 |
| <i>E</i> ₆ (reflectivity) ^(e) | | 9.1 | 11.2 | 12.5 | 13.9 |
| Experimental Electroreflectivity Peaks ^(h) | 2.0, 2.2, 2.5, 2.8 | 1.3, 1.4, 1.9, 2.2 | 1,18-1.25, 1.6, 2.2, 3.5 | 1.53, 1.78, 2.05, 3.0, 3.3, 3.8, 4.6 | 1.85, 1.98, 2.3-2.4, 3.3, 3.7, 4.0, 4.6 |

^(a) First-principles relativistic OPW solutions are listed in the *E* (REL) columns. All *E* (REL) entries except those in parentheses are based on Slater exchange. The *E* (REL) entries in parentheses are based on Kohn-Sham exchange. Experimental room temperature values are listed in the EXPT columns. Provisional

electroreflectivity peak assignments are shown in the EXPT columns in parentheses.

^(b) The double group symmetry symbols follow the conventions of Ref. [23]. The band number is indicated in parentheses. The highest valence band is denoted by (5), and the lowest

the Δ -type transitions are probably more important than the Σ - and L -type transitions.

In examining Cardona and Greenaway's E_1 , E_2 and E_3 values for the IV-VI compounds, Prakash [2] noted that these values are approximately in the ratio of 1 : 2 : 3 in most cases, but could not see any particular significance to the exactness of this ratio. In our view, the rough 1 : 2 : 3 ratio for E_1 , E_2 and E_3 in SnTe, PbTe, PbSe and PbS arises from the following two considerations: first, the interband separations between bands 4 and 5, 5 and 6, and 6 and 7 are nearly equal in the vicinity of the Σ saddle points in these materials; and second, interband transitions in this vicinity play an important role in establishing the E_1 , E_2 and E_3 reflectivity peaks, as noted in the preceding three paragraphs.

The E_4 structure (weak reflectivity peak) appears to arise from bands 4 and 5 \rightarrow band 6 transitions near X and along adjoining part of the Δ axis. Going by the correlation between theory and experiment (cf. table IV), we would place the 6.2 rather than the 5.4 eV peak in GeTe in the E_4 family.

The E_5 structure (weak reflectivity peak) appears to arise from several types of interband transitions, including band 3 \rightarrow bands 9, 10 and 11 and band 2 \rightarrow band 6 near the center of the zone, and band 3 \rightarrow band 6 near the X points. The correlation between theory and experiment (cf. table IV) suggests that in GeTe, the 7.8 rather than the 6.2 eV peak belongs to the E_5 family.

We have not reached any definite conclusions regarding the origin of the E_6 structure (weak peaks at higher energies). However, the rise in reflectivity above 15 eV in the lead salts can be attributed to transitions from filled d bands to various conduction bands, as suggested by CG. (This suggestion is consistent with the location of the cation d bands, as can be seen from table III.)

Electroreflectivity Spectra. If we take the position that electroreflectivity (ER) peaks are associated with

critical-point transitions, we are faced with the perplexing problem of having to relate the rich ER spectra of the IV-VI compounds, as measured by Aspnes and Cardona [35, 36] (see also Seraphin [37]), to the even richer assortment of critical-point transitions that our band calculations reveal at Γ , X , L , and W , along the Σ and Δ axes, and at more general points in the zone. If there is really an ER peak (including satellite structure) associated with each of the critical-point transitions, where are the missing ER peaks?

It is possible to associate many of the experimental ER peaks with the more obvious and familiar critical-point transitions, but it is quite difficult to establish the uniqueness of these associations, at least within the framework of available experimental and theoretical information.

To the extent that our own band calculations approximate the experimental situation, provisional assignments of some ER peaks can be made. These assignments are shown in parentheses in the EXPT columns of table IV. The E_1 -type ER peaks in PbTe (1.18 to 1.25 eV), PbSe (1.53 eV), and PbS (1.85 eV) are tentatively identified with $\Sigma_5(6) - \Sigma_5(5)$, that is to say, with band 5 \rightarrow band 6 transitions at the Σ saddle point. The next set of ER peaks [1.6 eV in PbTe; 1.78 eV in PbSe; and 1.98 eV in PbS] are tentatively identified with $L_6^-(7) - L_6^+(5)$. While some of these assignments are identical to those made previously by Aspnes and Cardona [35] (who based their analysis on the pioneering pseudopotential band calculations of Lin and Kleinman [10]), we depart from Aspnes and Cardona in some important particulars. For example, we do not regard the 1.53 and 1.78 eV ER peaks in PbSe, or the 1.85 and 1.98 eV ER peaks in PbS, as a doublet associated with the spin-orbit split L_3 valence band levels.

In the case of PbS, our calculations show that the L_3 spin-orbit splitting is 0.04 eV (cf. table II), while the experimental separation is considerably larger (0.13 eV). In the case of PbSe, our calculated L_3 spin-orbit

conduction band by (6). The Σ and Δ transitions refer to the saddle point transitions along the Σ and Δ axes. The theoretical E (REL) values for the Σ and Δ transitions are uncertain by about 0.1 to 0.2 eV (in some cases) because they were obtained by interpolation, rather than by direct calculation.

(^g) References [31] and [32].

(^h) SCANLON (W. W.), *J. Phys. Chem. Solids*, 1959, **8**, 423, and also Refs. [1] and [2].

(ⁱ) Reference [33]. Note that we are comparing our theoretical results with reflectivity spectra, rather than with ϵ_2 spectra, which are more closely related to the band structure. It should be borne in mind that corresponding reflectivity and ϵ_2 peaks may be displaced from one another by a few tenths of an eV, and, moreover, that the critical point transitions listed may lie a few

tenths of an eV above or below the corresponding ϵ_2 peaks. To call attention to these possible energy displacements, we have placed related theoretical and experimental values in different rows (These remarks do not apply to E_0 .)

(^j) Because of the switchover of L_6^+ and L_6^- in SnTe, the E (REL) entries for SnTe in this section have been keyed to the band indices rather than to the symmetry symbols.

For complete consistency of notation, the reader should interchange the symbols L_6^+ and L_6^- associated with bands 5 and 6 in SnTe. (These remarks do not apply to E_0 .)

(^k) In Ref. [33], the 6.2 and 7.8 eV reflectivity peaks in GeTe are associated with E_5 and E_6 rather than with E_4 and E_3 , as here.

(^l) References [35] and [36].

splitting (0.22 eV) is within striking distance of the experimental separation (0.25 eV), but our calculated transition energies (2.19 and 2.41 eV) are considerably larger than the experimental ER peaks energies (1.53 and 1.78 eV). If our interpretation is correct, the members of apparent spin-orbit split doublets in PbSe and PbS are actually associated with critical point transitions of nearly equal energy at different points in the zone (Σ saddle point and L).

The critical point transitions associated with the main reflectivity peak (E_2) in table IV may account for such ER peaks as the following: 2.0 and 2.2 eV in GeTe; 1.9 and 2.2 eV in SnTe; 2.2 eV in PbTe; 3.0 and 3.3 eV in PbSe; and 3.7 and 4.0 eV in PbS. These tentative assignments provide improved estimates of key critical point transition energies. More incisive interpretations of experimental reflectivity and electroreflectivity spectra await the completion of refined energy band and optical spectrum calculations now in progress [13].

IX. Concluding remarks. — To recapitulate, provisional energy band pictures have been obtained for GeTe, SnTe, PbTe, PbSe, and PbS by carrying out relativistic OPW band calculations at key points in the reduced zone, and then mapping out the band structure in the remainder of the zone with the aid of an interpolation scheme. These first-principles energy band calculations lead to physically realistic band models which are sufficiently accurate to account for most of the characteristic features of the experimental reflectivity spectra. It is difficult to interpret the electroreflectivity spectra unambiguously, but a number of plausible spectral assignments can be made. By comparing our provisional band pictures with the experimental evidence, improved estimates have been obtained for some key interband transition energies. These estimates are currently being used in refined energy band and optical spectrum calculations [13]. It is anticipated that these refined calculations will provide more incisive interpretations of reflectivity and electroreflectivity spectra, as well as more precise information about the effective masses and other band edge parameters.

X. Acknowledgment. — The authors wish to thank Dr. Edmund C. Burke for his encouragement; Professor Marvin L. Cohen, Dr. Kermit F. Cuff, Professor Walter A. Harrison, and Professor William Paul for many stimulating discussions; and Dr. David E. Aspnes, Professor Manuel Cardona, Professor Marvin L. Cohen, and Dr. Leo Esaki for sending copies of their papers in advance of publication.

Appendix

RELATIVISTIC OPW METHOD

The OPW matrix elements. — The OPW formalism can be directly extended to the use of relativistic wave functions [25]. We must use the 4-component solutions of the Dirac equation for both the plane waves and the atomic core states. We will assume a Slater-type exchange approximation. In Rydberg units the Dirac crystal Hamiltonian is

$$H = -\frac{2}{\alpha} \hat{\alpha} \cdot \nabla + \frac{2}{\alpha^2} \hat{\beta} + V(\mathbf{r})$$

where $\hat{\alpha}$ and $\hat{\beta}$ are 4×4 matrices [39], α is the fine structure constant, and $V(\mathbf{r})$ is a superposition of atomic potentials centered on lattice sites $\mathbf{R} = \mathbf{d} + \mathbf{f}$:

$$V(\mathbf{r}) = \sum_{\mathbf{d}, \mathbf{f}} V_{\mathbf{f}}(\mathbf{r} - \mathbf{d} - \mathbf{f}).$$

Let $|\mu, s\rangle$ be a plane wave spinor with wave vector μ , reduced wave vector \mathbf{k} , energy

$$E(\mu) = \frac{2}{\alpha^2} \sqrt{1 + (2\pi\mu\alpha)^2},$$

and spin s . Let $|\alpha, \mathbf{k}\rangle$ be a tight-binding combination of non-overlapping relativistic core wave functions characterized by $\alpha = \{n, l, j, m, \mathbf{f}\}$, energy E_α , and reduced wave vector \mathbf{k} . Then the inner product of these two vectors is the orthogonality coefficient

$$A_\alpha(\mu, s) = \langle \alpha, \mathbf{k} | \mu, s \rangle.$$

An orthogonalized plane wave is just the plane wave minus the projection of all core states:

$$|\mu, \mathbf{k}, s\rangle = |\mu, s\rangle - \sum_{\alpha}^{\text{core}} A_\alpha(\mu, s) |\alpha, \mathbf{k}\rangle.$$

One can immediately write down the expressions for the Hamiltonian and overlap matrix elements between two OPW's under the assumption that the core states are eigenfunctions of the crystal Hamiltonian

$$\begin{aligned} \langle \mu', \mathbf{k}, s' | H | \mu, \mathbf{k}, s \rangle &= \\ &= \langle \mu', s' | H | \mu, s \rangle - \sum_{\alpha}^{\text{core}} A_\alpha^*(\mu', s') A_\alpha(\mu, s) E_\alpha \\ \langle \mu', \mathbf{k}, s' | J | \mu, \mathbf{k}, s \rangle &= \\ &= \delta_{\mu', \mu} \delta_{s', s} - \sum_{\alpha}^{\text{core}} A_\alpha^*(\mu', s') A_\alpha(\mu, s). \end{aligned}$$

Evaluation of the orthogonality coefficients. — The evaluation of the orthogonality coefficients is straightforward but tedious. In our notation, a plane wave spinor with wave vector $\boldsymbol{\mu}$ and spin s is a positive energy solution of the Dirac equation with zero potential

$$|\boldsymbol{\mu}, s\rangle = \frac{1}{\Omega^{1/2}} u^{(s)}(\boldsymbol{\mu}) \exp(2\pi i \boldsymbol{\mu} \cdot \mathbf{r})$$

$$u^{(s)}(\boldsymbol{\mu}) = \begin{pmatrix} \sqrt{\frac{E(\mu) + 2/\alpha^2}{2E(\mu)}} \chi^{(s)} \\ \sqrt{\frac{E(\mu) - 2/\alpha^2}{2E(\mu)}} \frac{\boldsymbol{\sigma} \cdot \boldsymbol{\mu}}{\mu} \chi^{(s)} \end{pmatrix}.$$

A core band wave function is a superposition of Dirac-Slater-type atomic wave functions, ideally calculated in the crystal potential spherically averaged around the atomic site in question

$$|\alpha, \mathbf{k}\rangle = \frac{1}{N^{3/2}} \sum_{\mathbf{d}} \exp(2\pi i \mathbf{k} \cdot \mathbf{d}) \psi_{\alpha}(\mathbf{r} - \mathbf{d} - \mathbf{f}).$$

The atomic wave function is of the form

$$\psi_{\alpha}(\mathbf{r}) = \begin{pmatrix} + \frac{G_{nljf}(r)}{r} \sqrt{\frac{j+m}{2j}} Y_{j-1/2}^{m-1/2}(\theta\varphi) \\ + \frac{G_{nljf}(r)}{r} \sqrt{\frac{j-m}{2j}} Y_{j-1/2}^{m+1/2}(\theta\varphi) \\ - \frac{iF_{nljf}(r)}{r} \sqrt{\frac{j+1-m}{2j+2}} Y_{j+1/2}^{m-1/2}(\theta\varphi) \\ + \frac{iF_{nljf}(r)}{r} \sqrt{\frac{j+1+m}{2j+2}} Y_{j+1/2}^{m+1/2}(\theta\varphi) \end{pmatrix}$$

for $j = l + 1/2$

$$\psi_{\alpha}(\mathbf{r}) = \begin{pmatrix} + \frac{G_{nljf}(r)}{r} \sqrt{\frac{j+1-m}{2j+2}} Y_{j+1/2}^{m-1/2}(\theta\varphi) \\ - \frac{G_{nljf}(r)}{r} \sqrt{\frac{j+1+m}{2j+2}} Y_{j+1/2}^{m+1/2}(\theta\varphi) \\ - \frac{iF_{nljf}(r)}{r} \sqrt{\frac{j+m}{2j}} Y_{j-1/2}^{m-1/2}(\theta\varphi) \\ - \frac{iF_{nljf}(r)}{r} \sqrt{\frac{j-m}{2j}} Y_{j-1/2}^{m+1/2}(\theta\varphi) \end{pmatrix}$$

for $j = l - 1/2, l \neq 0$.

G and F are the large and small components of the radial wave function and satisfy

$$\frac{\alpha}{2} \left[E - \frac{2}{\alpha^2} - V_f(r) \right] G_{nljf}(r) = - \frac{dF_{nljf}(r)}{dr} + \frac{\kappa}{r} F_{nljf}(r)$$

$$\frac{\alpha}{2} \left[E + \frac{2}{\alpha^2} - V_f(r) \right] F_{nljf}(r) = \frac{dG_{nljf}(r)}{dr} + \frac{\kappa}{r} G_{nljf}(r)$$

$$\kappa = \begin{matrix} -(j+1/2) & \text{for } j = l+1/2 \\ (j+1/2) & \text{for } j = l-1/2. \end{matrix}$$

The orthogonality coefficient is

$$\begin{aligned} A_{\alpha}(\boldsymbol{\mu}, s) &= \langle \alpha, \mathbf{k} | \boldsymbol{\mu}, s \rangle \\ &= \frac{1}{N^{3/2} \Omega^{1/2}} \sum_{\mathbf{d}} \exp(2\pi i \mathbf{k} \cdot \mathbf{d}) \times \\ &\quad \times \int \psi_{\alpha}^*(\mathbf{r} - \mathbf{d} - \mathbf{f}) u^{(s)}(\boldsymbol{\mu}) \exp(2\pi i \boldsymbol{\mu} \cdot \mathbf{r}) d\mathbf{r}. \end{aligned}$$

A simple change of variables gives

$$\begin{aligned} A_{\alpha}(\boldsymbol{\mu}, s) &= \frac{1}{\Delta^{1/2}} \exp(2\pi i \boldsymbol{\mu} \cdot \mathbf{f}) \times \\ &\quad \times \int \psi_{\alpha}^*(\mathbf{r}') u^{(s)}(\boldsymbol{\mu}) \exp(2\pi i \boldsymbol{\mu} \cdot \mathbf{r}') d\mathbf{r}'. \end{aligned}$$

The integral is evaluated by expanding the plane wave in spherical harmonics and Bessel functions, using orthogonality to carry out the angular integration, and recursion relations among the spherical harmonics to collect the terms. With the following definition for the radial integrals

$$\begin{aligned} C_{nl\pm\frac{1}{2}f}(\mu) &= \sqrt{\frac{E(\mu) + 2/\alpha^2}{2E(\mu)}} \times \\ &\quad \times \int_0^{\infty} G_{nl\pm\frac{1}{2}f}(r) j_l(2\pi\mu r) r dr \\ &\quad \mp \sqrt{\frac{E(\mu) - 2/\alpha^2}{2E(\mu)}} \times \\ &\quad \times \int_0^{\infty} F_{nl\pm\frac{1}{2}f}(r) j_{l\pm 1}(2\pi\mu r) r dr \end{aligned}$$

the orthogonality coefficients take on a form very similar to the non relativistic case

$$\begin{aligned} A_{nljm_f}(\boldsymbol{\mu}, \pm) &= \frac{1}{\Delta^{1/2}} \exp(2\pi i \boldsymbol{\mu} \cdot \mathbf{f}) 4\pi i^l \times \\ &\quad \times \sqrt{\frac{j \pm m}{2j}} Y_{j-1/2}^{m\mp 1/2*}(\theta_{\boldsymbol{\mu}}, \varphi_{\boldsymbol{\mu}}) C_{nl\pm\frac{1}{2}f}(\mu) \end{aligned}$$

for $j = l + 1/2$

$$\begin{aligned}
 A_{nljm_f}(\boldsymbol{\mu}, \pm) &= \pm \frac{1}{A^{1/2}} \exp(2\pi i \boldsymbol{\mu} \cdot \mathbf{f}) 4\pi i^l \times \\
 &\times \sqrt{\frac{j+1 \mp m}{2j+2}} Y_{j+1/2}^{m \mp 1/2*}(\theta_{\boldsymbol{\mu}}, \varphi_{\boldsymbol{\mu}}) C_{nl l - \frac{1}{2}f}(\boldsymbol{\mu}) \\
 &\text{for } j = l - 1/2, \quad l \neq 0.
 \end{aligned}$$

The only difference comes from the projection of the spin of the plane wave on the spin of the atomic wave function.

The next step is to carry out the sums over m in the Hamiltonian matrix element. This is done with the use

$$\begin{aligned}
 \langle \boldsymbol{\mu}', \mathbf{k}, s' | H | \boldsymbol{\mu}, \mathbf{k}, s \rangle &= E(\boldsymbol{\mu}) \delta_{\boldsymbol{\mu}', \boldsymbol{\mu}} \delta_{s', s} + \\
 &+ \delta_{s', s} V(\boldsymbol{\mu}' - \boldsymbol{\mu}) \left[\sqrt{\frac{E(\boldsymbol{\mu}) + 2/\alpha^2}{2E(\boldsymbol{\mu})}} \sqrt{\frac{E(\boldsymbol{\mu}') + 2/\alpha^2}{2E(\boldsymbol{\mu}')}} + \cos \theta(\boldsymbol{\mu}', \boldsymbol{\mu}) \sqrt{\frac{E(\boldsymbol{\mu}) - 2/\alpha^2}{2E(\boldsymbol{\mu})}} \sqrt{\frac{E(\boldsymbol{\mu}') - 2/\alpha^2}{2E(\boldsymbol{\mu}')}} \right] \\
 &- \delta_{s', s'} \frac{4\pi}{A} \sum_{\mathbf{f}} \exp[2\pi i(\boldsymbol{\mu} - \boldsymbol{\mu}') \cdot \mathbf{f}] \sum_{\mathbf{l}}^{\text{core}} \left\{ (l+1) P_l[\cos \theta(\boldsymbol{\mu}', \boldsymbol{\mu})] \sum_n^{\text{core}} [E_{nl l + \frac{1}{2}f} C_{nl l + \frac{1}{2}f}(\boldsymbol{\mu}) C_{nl l + \frac{1}{2}f}(\boldsymbol{\mu}')] \right. \\
 &+ l P_l[\cos \theta(\boldsymbol{\mu}', \boldsymbol{\mu})] \sum_n^{\text{core}} [E_{nl l - \frac{1}{2}f} C_{nl l - \frac{1}{2}f}(\boldsymbol{\mu}) C_{nl l - \frac{1}{2}f}(\boldsymbol{\mu}')] \left. \right\} \\
 &+ i \frac{\boldsymbol{\mu}' \times \boldsymbol{\mu}}{\boldsymbol{\mu}' \boldsymbol{\mu}} \cdot \langle s' | \boldsymbol{\sigma} | s \rangle \left\{ V(\boldsymbol{\mu}' - \boldsymbol{\mu}) \sqrt{\frac{E(\boldsymbol{\mu}) - 2/\alpha^2}{2E(\boldsymbol{\mu})}} \sqrt{\frac{E(\boldsymbol{\mu}') - 2/\alpha^2}{2E(\boldsymbol{\mu}')}} \right. \\
 &+ \frac{4\pi}{A} \sum_{\mathbf{f}} \exp[2\pi i(\boldsymbol{\mu} - \boldsymbol{\mu}') \cdot \mathbf{f}] \sum_{\mathbf{l}}^{\text{core}} P'_l[\cos \theta(\boldsymbol{\mu}', \boldsymbol{\mu})] \\
 &\left. \times \sum_n^{\text{core}} [E_{nl l + \frac{1}{2}f} C_{nl l + \frac{1}{2}f}(\boldsymbol{\mu}) C_{nl l + \frac{1}{2}f}(\boldsymbol{\mu}') - E_{nl l - \frac{1}{2}f} C_{nl l - \frac{1}{2}f}(\boldsymbol{\mu}) C_{nl l - \frac{1}{2}f}(\boldsymbol{\mu}')] \right\}
 \end{aligned}$$

where

$$P'_l(\cos \theta) \text{ denotes } \frac{dP_l(\cos \theta)}{d \cos \theta}.$$

The overlap matrix element is similar, except it has no terms involving $V(\boldsymbol{\mu}' - \boldsymbol{\mu})$, and the energies are all replaced by 1. $V(\boldsymbol{\mu}' - \boldsymbol{\mu})$ is the Fourier transform of the full crystal potential and comes from the plane wave — plane wave part of the matrix element. The valence and conduction energy levels are the eigenvalues of the matrix equation.

$$|H - JE| = 0.$$

Note added in proof. — In this paper we have been concerned primarily with the overall band structure of the IV-VI compounds, rather than with the detailed shape of the valence and conduction band edges. In view of the difficulties that many workers have encountered in attempting to determine the

of identities among the spherical harmonics such as

$$\begin{aligned}
 \sum_{m=-l}^l \frac{l+m+1}{2l+1} Y_l^{m*}(\theta_{\boldsymbol{\mu}}, \varphi_{\boldsymbol{\mu}}) Y_l^m(\theta_{\boldsymbol{\mu}'}, \varphi_{\boldsymbol{\mu}'}) &= \\
 = \left\{ l+1 - i \left(\frac{\boldsymbol{\mu}' \times \boldsymbol{\mu}}{\boldsymbol{\mu}' \boldsymbol{\mu}} \right)_z \frac{d}{d \cos \theta(\boldsymbol{\mu}', \boldsymbol{\mu})} \right\} \times \\
 \times \frac{1}{4\pi} P_l[\cos \theta(\boldsymbol{\mu}', \boldsymbol{\mu})].
 \end{aligned}$$

When all the terms have been collected the resulting expression for the Hamiltonian matrix element is

exact nature of the principal and subsidiary band edges in these materials, it might not be out of place for us to make the following observations :

(a) As can be seen from figs. 1 through 5, there are apparent valence band maxima and conduction band minima along the Δ and Σ axes. As already mentioned on p. 71, these maxima and minima are not necessarily absolute extrema. In SnTe, for example, these maxima and minima actually define saddle points. Accordingly, the Δ and Σ maxima and minima are not necessarily subsidiary band edges in the same sense that the [100] conduction band minima in GaAs are, for example. This possibility should be borne in mind in analyzing optical and electronic transport data.

(b) In some of the IV-VI compounds, the Δ and Σ saddle points may lie only a few tenths of an eV

below or above the principal valence and conduction band edges at L. Since there will be ridges in the valence band between the Δ and Σ saddle points on the one hand, and the L point on the other, the surfaces of constant energy will change from a simple ellipsoidal shape to a highly fluted or warped shape as one moves away from the L point. (Similar remarks can be made for the conduction band.) In order to account for some of the transport measurements, it may be necessary to treat the valence and conduction band edges in terms of constant energy surfaces which are ellipsoidal in the immediate vicinity of L, but which rapidly assume a warped form as one moves away from L.

References

- [1] PUTLEY (E. H.), in *Materials Used in Semiconductor Devices*, edited by C. A. Hogarth (Interscience Publishers, New York, 1965), p. 71.
- [2] PRAKASH (V.), Division of Engineering and Applied Physics, Harvard University, Technical Report No HP-13, June 1967 (unpublished).
- [3] DIMMOCK (J. O.) and WRIGHT (G. B.), *Phys. Rev.*, 1964, **135**, A 821.
- [4] CUFF (K. F.), ELLETT (M. R.), KUGLIN (C. D.) and WILLIAMS (L. R.), *Proceedings of the International Conference on the Physics of Semiconductors, Paris*, 1964 (Dunod, Paris, 1964), p. 677.
- [5] MITCHELL (D. L.) and WALLIS (R. F.), *Phys. Rev.*, 1966, **151**, 581.
- [6] JOHNSON (L. E.), CONKLIN (J. B.), Jr., and PRATT (G. W.), Jr., *Phys. Rev. Letters*, 1963, **11**, 538.
- [7] CONKLIN (J. B.), Jr., JOHNSON (L. E.) and PRATT (G. W.), Jr., *Phys. Rev.*, 1965, **137**, A 1282.
- [8] FERREIRA (L. G.), *Phys. Rev.*, 1965, **137**, A 1601.
- [9] RABII (S.), *Phys. Rev.*, 1968, **167**, 801 ; **173**, 918.
- [10] LIN (P. J.) and KLEINMAN (L.), *Phys. Rev.*, 1966, **142**, 478.
- [11] LIN (P. J.), SASLOW (W.) and COHEN (M. L.), *Solid State Communications*, 1967, **5**, 893.
- [12] COHEN (M. L.), TUNG (Y.) and ALLEN (P. B.), this volume (Session C2).
- [13] HERMAN (F.) and VAN DYKE (J. P.), to be published.
- [14] HERMAN (F.), KORTUM (R. L.), KUGLIN (C. D.) and SHORT (R. A.), in *Quantum Theory of Atoms, Molecules, and the Solid State*, edited by P. O. Löwdin (Academic Press, New York, 1966), p. 381.
- [15] HERMAN (F.), KORTUM (R. L.), KUGLIN (C. D.) and SHORT (R. A.), *J. Phys. Soc. Japan*, 1966, **21**, 7. (Kyoto Conference Supplement.)
- [16] HERMAN (F.), KORTUM (R. L.) and KUGLIN (C. D.), *Intern. J. Quantum Chemistry*, 1967, **1S**, 533. (Sanibel Island Symposium Issue.)
- [17] SHAY (J. L.), SPICER (W. E.) and HERMAN (F.), *Phys. Rev. Letters*, 1966, **18**, 649.
- [18] HERMAN (F.), KORTUM (R. L.), KUGLIN (C. D.) and SHAY (J. L.), in *II-VI Semiconducting Compounds*, 1967 International Conference, edited by D. G. Thomas (W. A. Benjamin, Inc., New York, 1967), p. 503.
- [19] HERMAN (F.), KORTUM (R. L.), KUGLIN (C. D.) and VAN DYKE (J. P.), in *Energy Bands in Metals and Alloys*, edited by J. T. Waber and L. H. Bennett (Gordon and Breach, New York, 1968), p. 19.
- [20] HERMAN (F.), KORTUM (R. L.), KUGLIN (C. D.) and VAN DYKE (J. P.), in *Methods in Computational Physics*, edited by B. Alder, S. Fernbach and M. Rotenberg (Academic Press, New York, 1968), Vol. 8, 193.
- [21] HERMAN (F.) and SPICER (W. E.), *Phys. Rev.*, 1968, **174**. [October 16 issue.]
- [22] HERMAN (F.), KUGLIN (C. D.), CUFF (K. F.) and KORTUM (R. L.), *Phys. Rev. Letters*, 1963, **11**, 541.
- [23] ELLIOTT (R. J.), *Phys. Rev.*, 1954, **96**, 266, 280.
- [24] LOUCKS (T. L.), *Augmented Plane Wave Method* (W. A. Benjamin, Inc., New York, 1967).
- [25] SOVEN (P.), *Phys. Rev.*, 1965, **137**, A 1706.
- [26] LIBERMAN (D.), WABER (J. T.) and CROMER (D. T.), *Phys. Rev.*, 1965, **137**, A 27.
- [27] HERMAN (F.) and SKILLMAN (S.), *Atomic Structure Calculations* (Prentice-Hall, Inc., Englewood Cliffs New Jersey, 1963).
- [28] BOYD (R. G.), LARSON (A. C.) and WABER (J. T.), *Phys. Rev.*, 1963, **129**, 1629. See also Ref. 26.
- [29] ANIMALU (A. O. E.), *Phil. Mag.*, 1966, **13**, 53 ; G. Weisz, *Phys. Rev.*, 1966, **149**, 504 ; SARAVIA (L. R.) and BRUST (D.), *Phys. Rev.*, to be published.
- [30] DIMMOCK (J. O.), MELNGAILIS (I.) and STRAUSS (A. J.), *Phys. Rev. Letters*, 1966, **16**, 1193.
- [31] ESAKI (L.), *J. Phys. Soc. Japan*, 1966, **21**, 589. [Kyoto Conference Supplement.]
- [32] TSU (R.), HOWARD (W. E.) and ESAKI (L.), *Phys. Res.*, 1968, **172**, 779.
- [33] CARDONA (M.) and GREENAWAY (D. L.), *Phys. Rev.*, 1964, **133**, A 1685.
- [34] SPICER (W. E.) and LAPEYRE (G. J.), *Phys. Rev.*, 1965, **139**, A 565 ; B. H. Sacks and SPICER (W. E.), *Bull. Amer. Phys. Soc.*, 1965, **10**, 598.
- [35] ASPNES (D. E.) and CARDONA (M.), *Phys. Rev.*, 1968, **173**, 714 (PbS, PbSe, PbTe).
- [36] ASPNES (D. E.) and CARDONA (M.), *Bull. Amer. Phys. Soc.*, 1968, **13**, 27 (GeTe, SnTe).
- [37] SERAPHIN (B. O.), this volume (Session B 2).
- [38] GOLDAK (J.), BARRETT (C. S.), INNES (D.) and YUDELIS (W.), *J. Chem. Phys.*, 1966, **44**, 3323 ; see also COHEN (M. H.), FALICOV (L. M.) and GOLIN (S.), *IBM Journal of Research and Development*, 1964, **8**, 215.
- [39] ROSE (M. E.), *Relativistic Electron Theory* (John Wiley and Sons, Inc., New York, 1961).